Electronic Structure of Q_A^- in Reaction Centers from *Rhodobacter sphaeroides*. I. Electron Paramagnetic Resonance in Single Crystals

R. A. Isaacson,* F. Lendzian,‡ E. C. Abresch,* W. Lubitz,‡ and G. Feher*
*Department of Physics, University of California, San Diego, La Jolla, CA 92093 USA, and ‡Max-Volmer-Institut für Biophysikalische und Physikalische Chemie, Technische Universtät Berlin, D-10623 Berlin, Germany

ABSTRACT The magnitude and orientation of the electronic g-tensor of the primary electron acceptor quinone radical anion, Q_A^-, has been determined in single crystals of zinc-substituted reaction centers of *Rhodobacter sphaeroides* R-26 at 275 K and at 80 K. To obtain high spectral resolution, EPR experiments were performed at 35 GHz and the native ubiquinone-10 (UQ_{10}) in the reaction center was replaced by fully deuterated UQ_{10}. The principal values and the direction cosines of the g-tensor axes with respect to the crystal axes *a, b, c* were determined. Freezing of the single crystals resulted in only minor changes in magnitude and orientation of the g-tensor. The orientation of Q_A^- as determined by the g-tensor axes deviates only by a few degrees ($\leq 8°$) from the orientation of the neutral Q_A obtained from an average of four different x-ray structures of *Rb. sphaeroides* reaction centers. This deviation lies within the accuracy of the x-ray structure determinations. The g-tensor values measured in single crystals agree well with those in frozen solutions. Variations in g-values between Q_A^-, Q_B^-, and UQ_{10} radical ion in frozen solutions were observed and attributed to different environments.

INTRODUCTION

In reaction centers of photosynthetic bacteria (bRCs) light-induced electron transfer starts from the excited primary donor, a bacteriochlorophyll dimer, and proceeds through a series of electron acceptors along the "active" A-branch to the quinones Q_A and Q_B, which are both magnetically coupled to a non-heme high spin Fe^{2+} (Deisenhofer and Michel, 1989; Feher et al., 1989). In bRCs of *Rhodobacter sphaeroides*, both Q_A and Q_B are ubiquinone-10 (UQ_{10}) molecules (Fig. 1), which, however, differ from each other in several respects. They have different redox potentials and act sequentially in the electron transport chain. Q_A accepts only one electron and does not become protonated, whereas Q_B can be doubly reduced and then protonated to form dihydroquinone (Okamura et al., 1982). The chemical behavior of the two quinones in the bRC is strongly influenced by the protein environment, which modifies their electronic structures to optimize the efficiency of the electron and proton transfer processes (Okamura and Feher, 1992; Shinkarev and Wraight, 1993).

Information about the electronic structure of Q_A^- and Q_B^- has been obtained by electron paramagnetic resonance (EPR) (Loach and Hall, 1972; Feher et al., 1972; Butler et al, 1984; Debus et al., 1986; Burghaus et al., 1993) and electron nuclear double resonance (ENDOR) (Lubitz et al., 1985; Feher et al., 1985) techniques. In most of these studies, the high spin Fe^{2+}, which is magnetically coupled to the quinones, was replaced with a diamagnetic divalent metal ion, e.g., Zn^{2+}. Replacement of Fe by other metal ions (e.g., Cu or Zn) has been accomplished either by growing the bacteria in media that are Fe depleted and enriched with other metals (Rutherford et al., 1985; Buchanan and Dismukes, 1987, Ferris, 1987) or by chemical exchange of Fe with other metals (Debus et al., 1986). It has been shown that Zn-bRCs exhibit electron transfer kinetics that are essentially the same as those of native iron-containing bRCs (Debus et al., 1986; Kirmaier et al., 1986), whereas in iron-free bRCs the electron transfer rates were found to be different from those in native bRCs (Kirmaier et al., 1986; Schelvis et al., 1992).

EPR experiments at 9 and 35 GHz were first performed on iron-depleted bRCs with the aim of identifying the then unknown first electron acceptor (Feher et al., 1972). The observed g-values were characteristic for semiquinone radical anions. At 9 GHz, $g_{eff} = 2.0046$. (Typical values for quinone radicals are given in Pederson, 1983.). At 35 GHz, Q_A^- was found to have approximately an axially symmetric g-tensor (Feher et al., 1972). More recently, the principal values of the electronic g-tensor were resolved for Q_A^- in frozen solutions of Zn-bRCs by EPR at 95 GHz (Burghaus et al., 1993). For Q_B^- the electronic g-tensor has, so far, not been determined.

The g-tensor of an organic π-radical, like a quinone radical, is an integral property of the electronic wave function. Its principal values are influenced by the spatial distribution of the orbital carrying the unpaired electron. Deviations from the free electron value ($g_e = 2.00232$) arise from spin orbit induced admixtures of other orbitals into the half-filled π^*-orbital (Atherton, 1993). This effect increases with increasing spin densities at heavier atoms (e.g., oxygen) due to their larger spin orbit coupling constants (Carrington and McLachlan, 1969). In quinone radicals the

Received for publication 30 January 1995 and in final form 22 May 1995.
Address reprint requests to Roger A. Isaacson, Department of Physics, University of California, San Diego, M/C 0319, 9500 Gilman Dr., La Jolla, CA 92093-0319. Tel.: 619–534-2505; Fax: 619–534-0173; E-mail: risaacson@ucsd.edu.

0006-3495/95/08/311/12 $2.00

principal components of the g-tensor are, therefore, strongly influenced by the spin densities at the carbonyl oxygens.

The orientation of the g-tensor axes with respect to the Zn-bRC cannot be obtained from frozen solution spectra. To gain this information, single crystals of Zn-bRCs are required. As the location of the tensor axes in the quinone molecule (see Fig. 1) is assumed to be known (Burghaus et al., 1993), the experimental determination of the g-tensor axes provides detailed information about the orientation of Q_A^- in the Zn-bRC. This orientation can then be compared with that of the neutral Q_A molecule obtained from x-ray crystallographic analyses of bRC single crystals of *Rb. sphaeroides* R-26 (Allen et al., 1988; Chang et al., 1991) and 2.4.1 wild-type bRCs (Chirino et al., 1994; Ermler et al., 1994). Furthermore, a comparison of the magnitudes of the g-tensor principal values of Q_A^- and Q_B^- in the Zn-bRC with that of UQ_{10}^- in organic solvents is expected to show effects due to different environments. For example, different hydrogen bonding to the carbonyl oxygens will influence the orbital energies and the spin-density distributions of these three species, thereby leading to different principal values of the g-tensor (Burghaus et al., 1993). Earlier ENDOR work (Lubitz et al., 1985; Feher et al., 1985) has shown that the electronic structure is indeed different for the three species. These differences have been attributed to the interaction of the quinone radical anions with their protein surrounding, e.g., by the formation of hydrogen bonds between specific amino acid residues and the carbonyl oxygens of the quinones (Allen et al., 1988; Chang et al., 1991; Ermler et al., 1994).

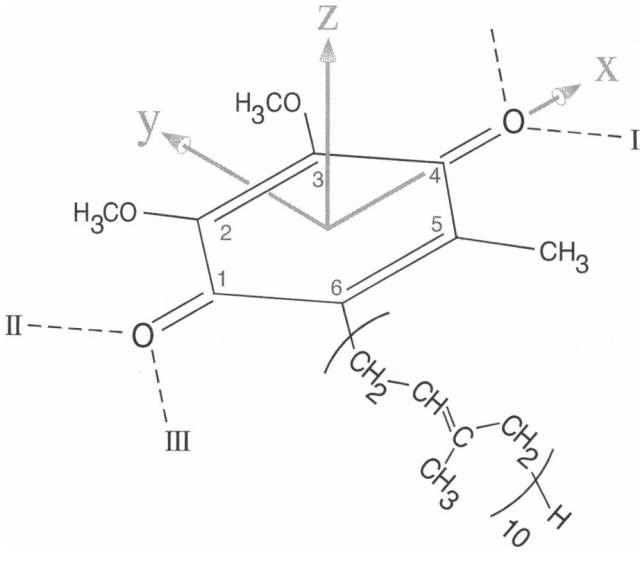

FIGURE 1 Molecular structure and numbering scheme for UQ_{10}. The carbonyl oxygens (O1, O4) are labeled according to the carbon atom to which they are attached. The molecular axis system (x, y, z) is colinear with the respective principal axes of the g-tensor (g_{xx}, g_{yy}, g_{zz}) of the radical anion (see text). The effect of hydrogen bonds on the direction of the g-tensor was simulated by two point charges (+0.5 e) placed along the direction of the oxygen lone pairs either at positions I and II or I and III (dashed lines) or by a single point charge or a single water molecule at position I. For details see text.

In this paper we report on the crystallization of Zn-bRCs of *Rb. sphaeroides* R-26 and the generation and stabilization of the primary quinone radical anion Q_A^-. In these crystals the g-tensor of Q_A^- was determined by EPR spectroscopy at 35 GHz, both at room temperature (275 K) and at 80 K. From these experiments the orientation of the singly reduced primary quinone in the Zn-bRC was obtained. Furthermore, the principal values of the electronic g-tensor for Q_A^- and Q_B^- were measured in frozen solutions of Zn-bRCs and compared with each other and with those found for UQ_{10}^- in organic solvents. A preliminary account of this has been presented by Isaacson et al. (1994).

MATERIALS AND METHODS

Preparation of reaction centers

RCs from *Rb. sphaeroides* R-26 were extracted and purified as previously described (Feher and Okamura, 1978) with the following modifications. Chromatophores were suspended in 15 mM Tris, 1mM EDTA, and 0.1 M NaCl at an optical absorption at 850 nm (A_{850}^{1cm}) of 50 (Wraight, 1979). They were treated with 0.5 to 0.7% lauryl dimethylamine oxide (LDAO) (Fluka, New York) for 10 min at room temperature and centrifuged for 2 h at 235,000 *g* at 4°C. After centrifugation, 1% w/v LDAO and 25% w/v ammonium sulfate were added to the RC supernatant and centrifuged again for 5 to 10 min at 12,000 *g*. The floating Zn-bRC pellets were stirred overnight in 15 mM Tris, 1 mM EDTA at 4°C. After a 30-min centrifugation at 40,000 *g* to remove unsolubilized material, Celite (Manville, Denver, CO) was added to the Zn-bRCs at 1 g/100 A_{800} V (ml). The Zn-bRC-Celite was packed into a Buchner funnel and washed with 25% ammonium sulfate w/v, 15 mM Tris, 1 mM EDTA, 0.1% LDAO until the filtrate was no longer colored. The Zn-bRCs were then eluted with 15% ammonium sulfate in 15 mM Tris, 1 mM EDTA, 0.1% LDAO. Ammonium sulfate was removed by passing the Zn-bRCs over a Sephadex G-25 (Pharmacia, Uppsala, Sweden) column equilibrated with 15 mM Tris, 1 mM EDTA, 0.1% LDAO. The desalted Zn-bRCs were then pumped onto a Fractogel-DEAE (EM Science, Gibbstown, NJ) column and eluted with a gradient of 0 to 0.3 M NaCl in 15 mM Tris, 1 mM EDTA, 0.1% LDAO. After dialysis, Zn-bRCs were further purified by (HPLC) with a Beckman 110B pump-based system equipped with an LKB 2138 UV detector Zn-bRCs were injected onto a PLSAX 1000 Å (20 μm) HPLC anion exchange column (1 cm × 20 cm) and then eluted with a linear gradient of 0 to 0.2 M NaCl in 15 mM Tris, 1 mM EDTA, 0.1% LDAO over 10 min at a flow rate of 2 ml/min. Fractions were collected every minute. All fractions with optical absorbance ratios of $A_{280}/A_{800} \leq 1.20$ were combined and dialyzed against 10 mM Tris, 0.1 mM EDTA, 0.025% LDAO. The yields were ~70% of the Zn-bRCs injected. Finally, the Zn-bRCs were concentrated to 100–300 μM by ultracentrifugation with an Amicon Centricon-30.

Deuteration of reaction centers

Fully deuterated Zn-bRCs were obtained by growing *Rb. sphaeroides* R-26 bacteria in a D_2O-based modified Hutner's medium using perdeuterated succinic acid (98% D, Aldrich, Milwaukee, WI) as the sole carbon source as described previously (van der Est et al., 1993). Zn-bRCs were then extracted and purified as described above.

Incorporation of Zn

For frozen solution samples, the removal of iron and incorporation of Zn^{2+} was accomplished chemically with the chaotropic salt LiSCN and *o*-

phenanthroline as previously described (Debus et al., 1986). The Zn content was determined by atomic absorption spectroscopy to ≥90%. These preparations didn't yield useable crystals. Consequently, for Zn-bRC crystal samples, the Zn^{2+} was incorporated biosynthetically. *Rb. sphaeroides* R-26 bacteria were grown in modified Hutner's medium containing a high concentration of zinc (40 ppm) and a low concentration of iron (0.03 ppm) (Ferris, 1987). Zn-bRCs were extracted and purified as described above. Zn-bRCs isolated from bacteria grown in this way contained 30% Zn (70% Fe) as determined by atomic absorption spectroscopy.

Deuteration of ubiquinone

To reduce the EPR line width and thereby improve the spectral resolution, UQ_{10} was deuterated. Deuterated UQ_{10} was extracted by standard procedures (Takamiya and Takamiya, 1969) from bacteria grown in D_2O (99%) with deuterated succinic acid as carbon source. The deuterated UQ_{10} was further purified by HPLC on a Licrosorb Si 60 column (300 × 3.2 mm, 5 μm; Alltech, Deerfield, IL) with methylene chloride as the mobile phase. It was eluted after approximately 5 min. UQ_{10} was replaced in Zn-enriched Zn-bRCs by fully deuterated UQ_{10} (95% incorporation) following the procedure of Okamura et al (1975). The reconstituted Zn-bRCs contained 1.5 ± 0.2 UQ_{10}/Zn-bRC as determined by photo-oxidation of cytochrome *c* (Okamura et al., 1982).

Crystallization of Zn-bRCs

Single crystals were grown from biosynthetically enriched Zn-bRCs by vapor diffusion as described by Allen and Feher (1991). The crystals were needle-shaped, up to 4–5 mm long and had a rhombic cross section with a width of 0.5–0.8 mm along their widest dimension. The morphology of the crystals together with the symmetry axes *a,b,c* of the unit cell is shown in Fig. 2 *a*. The crystal space group is $P2_12_12_1$ with four molecules (sites) per unit cell. The crystals were soaked in D_2O artificial mother liquor for 48 h at room temperature to replace all exchangeable protons in the surroundings of the quinone that could contribute to hyperfine broadening of the EPR signal.

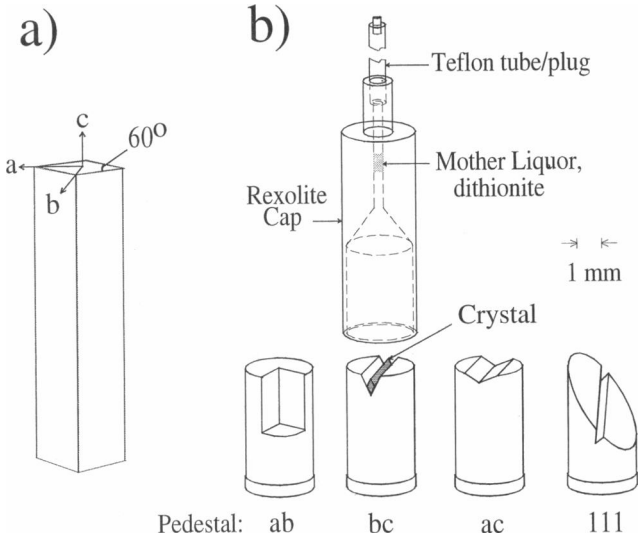

FIGURE 2 (*a*) Morphology of the orthorhombic reaction center single crystals (space group $P2_12_12_1$). The crystal axes *a*, *b*, and *c* (needle axis) are shown. Note that the angles between the outer crystal surfaces are 60° and 120°. (*b*) Pedestals with appropriate V-shaped grooves for aligning the crystal in the magnetic field B_0. The *a-b* and *a-c* plane pedestals have 120° grooves and the *b-c* and (1,1,1)-plane pedestals have 60° grooves to match the external crystal faces. Rotation of the crystal in the magnetic field B_0 is then either around the *c*, *a*, or *b* axis. For the (1,1,1) pedestal, rotation is in a plane connecting the respective 45° (135°) orientation of B_0 in the *a-b*, *a-c*, and *b-c* planes (see text and Fig. 6 for details). The placement of the crystal is shown for the *b-c* plane pedestal as an example. The pedestal and cap are flushed with argon and the crystal is reduced with dithionite solution. After removal of most of the solution, the crystal is protected from oxygen by the Rexolite cap sealed with high vacuum silicone grease. The teflon tube is sealed with a greased plug.

Generation of semiquinone radical anions in single crystals and solutions

The semiquinone anion radical Q_A^- was produced in Zn-bRC single crystals by chemical reduction rather than illumination to avoid interference from other paramagnetic species (e.g., the primary donor cation radical and secondary acceptor Q_B^-). The mother liquor around the crystal was replaced with a 0.3 M $Na_2S_2O_4$/1 M Tris solution (prepared in mother liquor under an argon atmosphere) for 60 s. After removal of most of the solution, the crystal was sealed off to exclude oxygen and placed in the EPR resonator. The half-life of Q_A^- in Zn-bRC single crystals at 275 ± 2 K was 2–5 h. This limited the data collection time, thereby imposing a limitation on the signal-to-noise ratio of the data taken near room temperature as compared with 80 K at which the radical lifetime was unlimited. For measurements at low temperature, the mounted and reduced single crystals were quickly frozen by immersing them into liquid nitrogen.

Frozen solution (powder) samples were made from fully deuterated Zn-bRCs that were concentrated to $A_{100}^{1\,cm} \approx 30$. Q_A^- was generated by illuminating the sample, in D_2O buffer, in the presence of a fivefold excess of cytochrome *c* (horse heart; Sigma Chemical Co., St. Louis, MO), with white light (500 W projection lamp/water filter) for 5 s followed by rapid freezing in liquid nitrogen. Reduction of Q_A in Zn-bRCs with dithionite instead of light has been shown earlier to give identical Q_A^- spectra (Lubitz et al., 1985; Feher et al., 1985). Q_B^- was generated in a similar way but with one saturating laser flash (0.3 J in 0.5 μs, Phase-R model DL2100C, Lumen-X Inc., New Durham, NH) in liquid solution at room temperature (excess of deuterated UQ_{10} added) followed by rapid freezing by immersion into liquid nitrogen. To obtain the quinone spectra in an organic solvent, fully deuterated UQ_{10} was converted to the semiquinone radical anion by dissolving the quinone in alkaline isopropanol-d_8 (98.5%; Sigma) under argon (Feher et al., 1985).

EPR instrumentation

The Q-band (35 GHz) EPR spectrometer is a home-built superheterodyne-type instrument with a standard Varian klystron, a cylindrical TE_{012} cavity, and an immersion dewar system for temperature control. The cavity was constructed from a fused quartz tube (12 mm outside diameter × 10 mm inside diameter). Silver paint (Dupont 4887) was sprayed on the inside surface and baked on at 600°C followed by electroplating with high purity silver. The unloaded Q was ~5000 at 80 K and ~2000 at 275 K. The microwave coupling to the cavity was achieved by an iris with a dipole antenna. The field modulation coils were mounted on the magnet pole faces, which facilitated experiments in which the magnet rather than the sample was rotated. This limited the field modulation frequency to ~400 Hz, which, however, did not introduce excess crystal detector noise as superheterodyne detection was used.

To obtain EPR data in the different crystallographic planes, the crystals were mounted on Rexolite (C-Lec Plastic Co., Beverly, NJ) pedestals having appropriate V-shaped grooves that aligned the crystals with respect to the magnetic field B_0 (for details see Fig. 2 *b*). EPR data in the *a-b* plane could also be obtained by mounting the crystal in a standard capillary tube with the long (*c*) axis of the crystal parallel to the axis of the capillary. A phosphorous-doped silicon (P-Si) powder sample was used as a g-marker (Stesmans and DeVos, 1986). Its g-value was determined from a calibration against a Li/LiF g-standard (Stesmans and Van Gorp, 1989) to be

1.99891 ± 0.00003 at T = 80 K. The P-Si marker was permanently mounted at the top surface of the cavity where the microwave field is radial and the EPR signal amplitude is a function of the angular position of the magnet. This provides a convenient way to control the amplitude of the marker; the magnet was set to the desired position and the sample rotated to obtain the angular dependence of the g-value of Q_A^-. The P-Si marker was usually measured together with the sample as a g-standard, as small changes in the microwave frequency may occur when the crystal is rotated in the cavity and small changes in B_o occur when the magnet is rotated. For measurements near room temperature the P-Si marker has limited accuracy due to line broadening and was therefore not used. Instead, the center of the B_o field sweep was periodically adjusted (manually) by using a model PT 2020 (Metrolab Instruments, Geneva, Switzerland) self-locking NMR Teslameter. For calibration of the B_o magnetic field sweep range, a Mn^{2+} powder sample (0.02% in MgO) was used as a g-marker (Low, 1957). The microwave frequency was measured with a model 548A (EIP Microwave, Milpitas, CA) frequency counter.

Independent control experiments on frozen solution samples were performed on a Bruker ER 200D EPR spectrometer equipped with a Bruker Q-band bridge, Bruker ER 5103 QTH resonator, and an Oxford CF935 cryostat. The results obtained were identical within experimental error to those measured with the Q-band EPR spectrometer described above.

Data were collected on a Nicolet (Madison, WI) 1180 minicomputer and transferred to a 486 PC for analysis and plotting. The EPR powder spectra were analyzed by using a simulation and fit program based on the work of Rieger (1982) that utilizes a Levenberg-Marquardt nonlinear least squares method (Press et al., 1988). Single-crystal EPR spectra were fitted with multiple Gaussian derivatives and decomposed with the commercial program Peakfit (version 3.15, Jandel Corp., San Rafael, CA).

RESULTS

EPR spectra of Q_A^- in single crystals were obtained in all three crystallographic planes of Zn-bRC. In Fig. 3, the four Q_A molecules in the unit cell are shown on an enlarged scale, projected onto the three crystallographic symmetry planes of the crystal (Chirino et al., 1994). For an arbitrary orientation of the crystal in the external magnetic field B_o, EPR signals from all four sites are obtained. If B_o lies in one of the principal crystallographic planes (*a-b*, *a-c*, or *b-c*), the sites are pairwise magnetically equivalent. When the external field is along any of the three principal crystallographic axes *a*, *b*, or *c*, all four sites are equivalent. Spectra were taken at 9 and 35 GHz; the use of the higher frequency and of Zn-bRC single crystals with perdeuterated UQ_{10} in D_2O buffer proved to be important to fully resolve the site splitting in the principal crystallographic planes. As an example, 35-GHz EPR spectra at 80 K in the *ab*-plane (crystal rotation around the needle axis *c*) for three different orientations are shown in Fig. 4. With the field axis B_o oriented along *a* or *b*, only one line is observed as all four sites are magnetically equivalent. With B_o making an angle of 45° with the *a* and *b* axes, two EPR lines are observed; they are assigned to the two inequivalent sites in the crystal (see Fig. 3). The measured linewidths are both 0.40 ± 0.02 mT. Single crystals in H_2O buffer exhibited approximately 50% larger linewidth. This shows that hyperfine interactions from protons in the vicinity of the quinone radical anion contribute significantly to the EPR linewidth.

The angular dependence of the apparent g-factor at 275 K and at 80 K obtained by rotating the magnetic field in the three crystallographic planes *a-b*, *a-c*, and *b-c* is shown in Fig. 5. Site splittings arising from the magnetic inequivalence of the sites are clearly resolved in all three planes. The g-tensor elements g_{ij} were obtained from fits (using Peakfit) to the linearized equation (see Klette et al., 1993).

$$g(\theta) = g_{ii}\cos^2\theta + g_{jj}\sin^2\theta + 2g_{ij}\sin\theta\cos\theta \qquad (1)$$

where the labels *i* and *j* denote pairs of crystal axes *a,b,c*, and θ is the angle between B_o and the *i* axis. The resulting nondiagonal g-tensor of Q_A^- at 80 K and near room temperature (275 ± 2 K) in the crystal axis system (*a,b,c*) is given in Table 1. These g-tensor elements are the results of

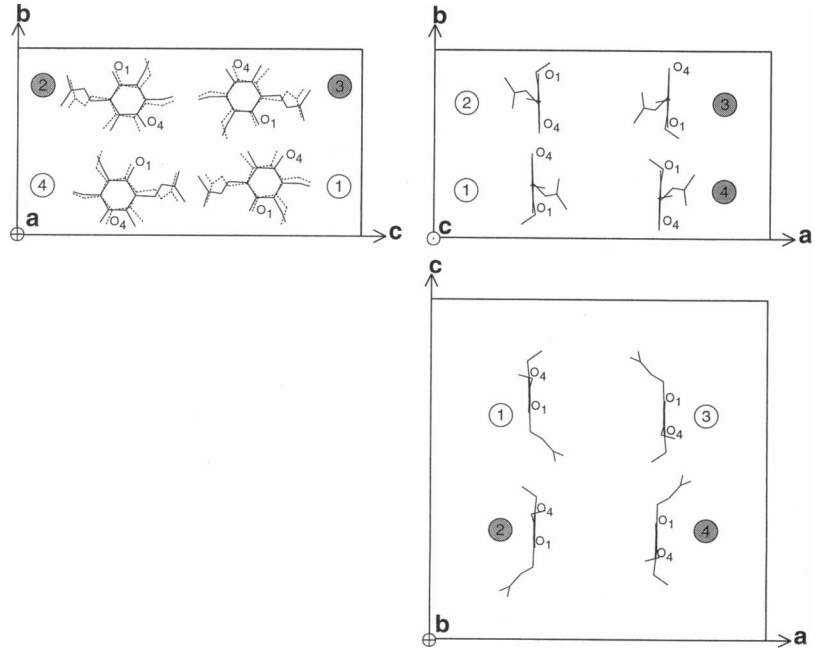

FIGURE 3 Relative orientation of the four Q_A molecules 1 to 4 (enlarged) in the unit cell of *Rb. sphaeroides* 2.4.1 bRCs projected onto the three symmetry planes of the crystal as obtained from x-ray crystallography (Chirino et al., 1994). Those pairs that have shaded labels are magnetically equivalent sites in each plane. Likewise, the unshaded labels are equivalent. Site 1 is the site for which the x-ray coordinates (Brookhaven Protein Data Bank, entry number 1PSS) are given. The other three sites are created mathematically by using the given crystal symmetry space group. Distances between the Q_A molecules are not to scale. The upper left panel (*b-c* plane) compares the position of the Q_A molecules obtained from two different crystal structure determinations: bRCs of *Rb. sphaeroides* R-26 (4RCR) and 2.4.1 (1PSS). Note that the Q_A molecules are rotated relative to each other by 12° and that the orientation of the substituents (isoprenoid chain and methoxy groups) is different. These differences are believed to be due to errors arising from the limited resolutions of the x-ray structure determination.

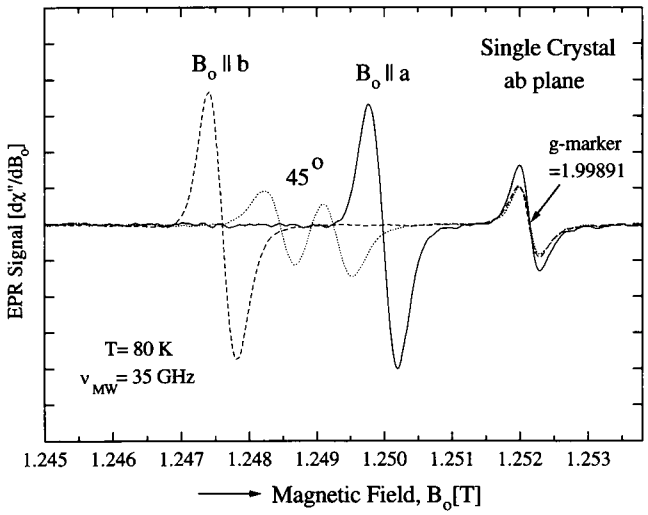

FIGURE 4 Q-band (35 GHz) EPR spectra of perdeuterated Q_A^- in a Zn-bRC single crystal for three different orientations in the *a-b* plane at 80 K. Single EPR lines are observed with B_o parallel to either symmetry axis *a* or *b*; along these axes all four sites in the unit cell are magnetically equivalent. At 45° two lines are observed, each belonging to a magnetically equivalent pair of sites (see Fig. 3). The spectrometer gain is the same for all three traces. The signal at g = 1.99891 is a phosphorous-doped silicon g-marker permanently mounted in the cavity. The marker amplitude is not constant for reasons explained in the text. Experimental conditions: microwave power = 3 μW; field modulation amplitude = 0.25 mT and frequency = 400 Hz; scan time = 30 s, two scans for each angle.

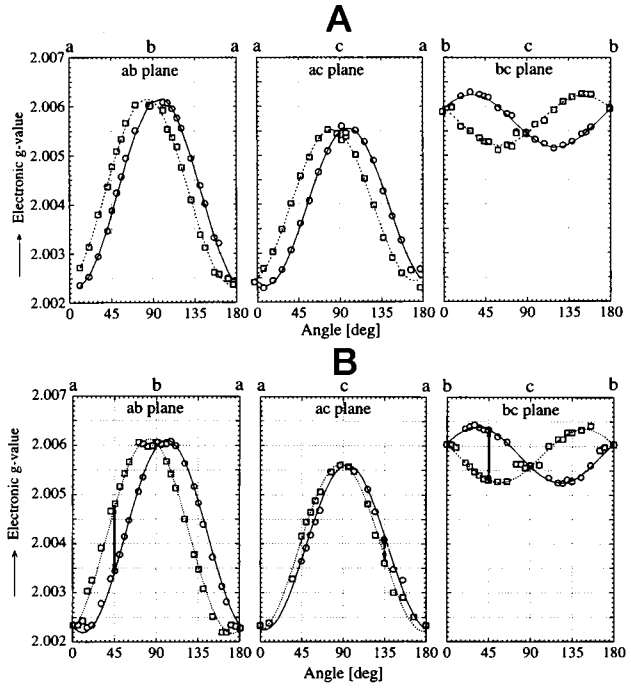

FIGURE 5 Angular dependence of the g-factor of Q_A^- in Zn-bRC single crystals at 275 K (*A*) and at 80 K (*B*), with rotation of the magnetic field B_o in the three crystallographic planes *a-b*, *a-c*, and *b-c*. Data for each plane were obtained from a different crystal. The curves presented were obtained from only one crystal per plane and consequently differ slightly from values given in the tables, which are averages of data from three different crystals. Solid lines represent fits to Eq. 1 for the two sets of pairwise equivalent sites in each plane marked by ○ and □, respectively. Site 1 (see Fig. 3) is represented by ○. The pairs of sites that are equivalent in the three symmetry planes are indicated in Fig. 3. The most prominent difference at 275 K as compared with 80 K is a larger site splitting in the *a-c* plane (for values see text).

averages of data obtained from three crystals for each plane. The values in parentheses of both g-matrices are estimated errors in the last digits obtained from the fitting procedure and from the experimentally observed variation between crystals. The estimated errors at 275 K are slightly less than for 80 K, despite the fact that the signal-to-noise ratio is larger at 80 K (because of higher Q, larger Boltzmann factor, and more data collected). The reason for this is the larger variations observed between different frozen crystals. These variations may be caused by structural differences introduced during the freezing procedure. The differences in the g-tensor at low and high temperature are discussed later.

There are eight possible sign combinations of the three off-diagonal elements g_{ij} ($i,j = a,b,c$). After diagonalization of the g-matrix, using all possible sign combinations for these elements, eight tensors are obtained. They can be grouped into two sets, A and B, each having four g-tensors. Within each set the four tensors have the same eigenvalues, but the signs of the direction cosines are different. The different sign combinations represent the four sites in the unit cell (see Fig. 3 and Klette et al., 1993). The four members of a set are related by the inversion of the signs of two elements, which corresponds to a rotation of 180°. For example, the transformation $a \rightarrow -a$, $b \rightarrow -b$, and $c \rightarrow c$ is a 180° rotation about the *c* axis and corresponds to a transformation from site 1 into site 2. Corresponding members of the different sets A and B are related by inversion of the sign of only one element g_{ij}. This does not correspond to a rotation but leads to a tensor with different principal values. The signs of the off-diagonal elements g_{ab}, g_{ac}, and g_{bc} and the signs of the direction cosines of the eigenvectors obtained by diagonalization are given in Table 2 for all eight tensors. (The assignment of the g-tensors to specific sites is discussed in a later section.) Tensors g_1, g_2, g_3, and g_4 belong to the same set (A); tensors g_1^*, g_2^*, g_3^*, and g_4^* belong to the second set (B). The tensors of sets A and B are both consistent with the rotation patterns in the symmetry planes. Because of the pairwise magnetic equivalence, the relative signs of the elements g_{ij} cannot be determined by EPR performed in one of the symmetry planes. To avoid this problem one needs to rotate the crystal about a non-symmetry, "skew" axis, where the EPR spectrum of all four sites are resolved (Atherton, 1993). From an analysis of the rotation pattern in this nonsymmetry plane, one can determine the relative signs of g_{ij} and eliminate the physically unreal set as described below.

A special pedestal was made for the above "skew" experiment. The crystal was mounted with its *b* axis parallel to a plane making an angle of 35° with respect to the rotation axis and with its *c* axis rotated 45° about the normal of this plane (see Fig. 2 *b*). For this pedestal B_0 is rotated in the

TABLE 1 g-Tensor of Q_A^- in the crystal axis system *a*, *b*, *c*

	T = 80 K			T = 275 K		
	a	*b*	*c*	*a*	*b*	*c*
a	+2.00232 (2)*	±0.00068 (10)	±0.00032 (7)	+2.00248 (2)	±0.00038 (7)	±0.00048 (3)
b	±0.00068 (10)	+2.00606 (3)	±0.00045 (3)	±0.00038 (7)	+2.00619 (3)	±0.00047 (3)
c	±0.00032 (7)	±0.00045 (3)	+2.00559 (2)	±0.00048 (3)	±0.00047 (3)	+2.00557 (2)

* Numbers in parentheses are errors in the last digit.

plane connecting the respective 45° (or 135°) orientations of the *a*-*b*, *a*-*c*, and *b*-*c* planes for which maximal site splittings occur (see Fig. 5). This (111) plane is defined by three points being the tips of unit vectors along each of the axes *a*, *b*, and *c* of the orthorhombic unit cell (points 1, 0, 0; 0, 1, 0; and 0, 0, 1). Fig. 6, *A* and *B*, shows the predicted angular dependence of the g-factor for a rotation in this plane for the two choices (set A and set B) calculated from the g-tensor at 80 K given in Table 1. The predicted patterns are quite different for the two sets (see in particular regions between 120° and 180° and around 90°). Comparison between the experimental rotation pattern using the (111) plane pedestal (Fig. 7) and the predicted patterns (Fig. 6, *A* and *B*) clearly shows that only tensor set A (g_1, g_2, g_3, and g_4) agrees with the calculated pattern. The eigenvalues and eigenvectors for g_1 and g_1* (for 80 K and 275 K) are given in Table 3. The tentative assignment of g_1 to site 1 in the unit cell is discussed below.

As a check of the single crystal results, EPR powder spectra were also taken. A comparison of the spectra at 35 GHz obtained from Q_A^- and Q_B^- in frozen Zn-bRCs and for UQ_{10}^- in frozen isopropanol-d_8 are shown in Fig. 8. To achieve the highest spectral resolution, all quinones were fully deuterated. All three species show differences in the positions of their g_{yy} and, in particular, g_{xx} components. The spectra were analyzed with a powder EPR simulation and fit program as described in the previous section. The principal values of the g-tensors are given in Table 4.

DISCUSSION

Inspection of Table 4 shows that the principal values of the electronic g-tensors obtained for Q_A^- in the Zn-bRC single crystal at Q-band agree well with those measured in frozen solutions at the same frequency and temperature (80 K). Comparison of these g-tensor values with earlier 95 GHz EPR data obtained from frozen Zn-bRC solution (Table 4) shows that the principal values agree within experimental error (±0.0001), although there seems to be a consistent shift of +0.0001 at 95 GHz as compared with the data at 35 GHz. It is not known at present whether this is due to a calibration problem or a real shift of the g-tensor values in different samples. A comparison of the g-tensor principal components of Q_A^-, Q_B^-, and UQ_{10}^- (Fig. 8) shows small but significant variations, in particular in the g_{xx} value (Table 4). It has been proposed (Burghaus et al., 1993) that this component, which lies along the quinone C-O bonds (see

TABLE 2 Combinations of signs of the off-diagonal elements g_{ij} and the direction cosines of the principal axes for tensors g_1 to g_4* (T = 80 K)[a]

	Set A				Set B			
	Site 1, g_1	Site 2, g_2	Site 3, g_3	Site 4, g_4	Site 1, g_1*	Site 2, g_2*	Site 3, g_3*	Site 4, g_4*
g_{ab}[b]	−	−	+	+	−	−	+	+
g_{ac}	−	+	−	+	+	−	+	−
g_{bc}	+	−	−	+	+	−	−	+
ℓ_{xa}[c]	−	+	+	−	−	+	+	−
ℓ_{xb}	+	−	+	−	+	−	+	−
ℓ_{xc}	+	+	−	−	+	+	−	−
ℓ_{ya}	+	−	−	+	+	−	−	+
ℓ_{yb}	−	+	−	+	−	+	−	+
ℓ_{yc}	+	+	−	−	+	+	−	−
ℓ_{za}	+	−	−	+	+	−	−	+
ℓ_{zb}	+	−	+	−	+	−	+	−
ℓ_{zc}	+	+	−	−	−	−	+	+

[a] At T = 275 K the eigenvector elements ℓ_{ya} of the tensors g_1–g_4 have inverted signs. These elements are near 90° so small angular deviations above and below 90° will give sign reversals. All other elements have the same signs.

[b] Signs of off-diagonal elements in crystal axis systems g_{ab}, g_{ac}, and g_{bc}. Set B can be eliminated on the basis of the experiments performed in the skew plane (1, 1, 1), see text and Figs. 6 and 7. The principal values of the g-tensors of sets A and B (sets with *) are given in Table 3.

[c] Signs of direction cosines $\ell_{xa} \ldots \ell_{zc}$ of the eigenvectors of the principal components g_{xx}, g_{yy} and g_{zz}.

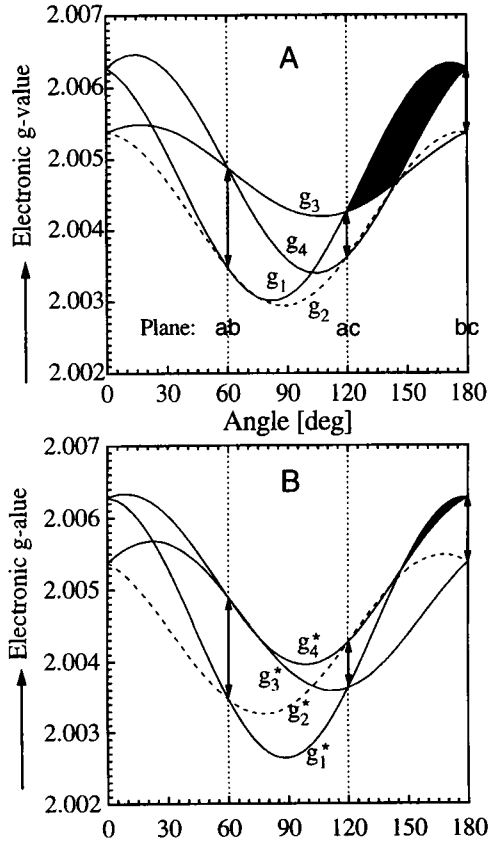

FIGURE 6 Calculated angular dependences of the g-tensor of Q_A^- in Zn-bRCs for the two sets A and B of g-tensors with the tensor elements of Table 1 (80 K) and the sign combinations given in Table 2 for rotation in the (1,1,1)-plane. Calculated pattern for tensor set g_1, g_2, g_3, g_4 (set A, top) and for tensor set g_1^*, g_2^*, g_3^*, g_4^* (set B, bottom). Regions of pronounced differences between sets A and B are shaded. Note that the experimental data of Fig. 7 agree only with the calculated pattern for tensor set A. Three two-headed arrows (also in Fig. 7) indicate the orientations for which B_o is in the crystal planes *a-b*, *a-c*, and *b-c*. The corresponding crystal orientations in Fig. 5 *B* are similarly marked for each of the three symmetry planes (45° for the *a-b* and *b-c* planes and 135° for the *a-c* plane).

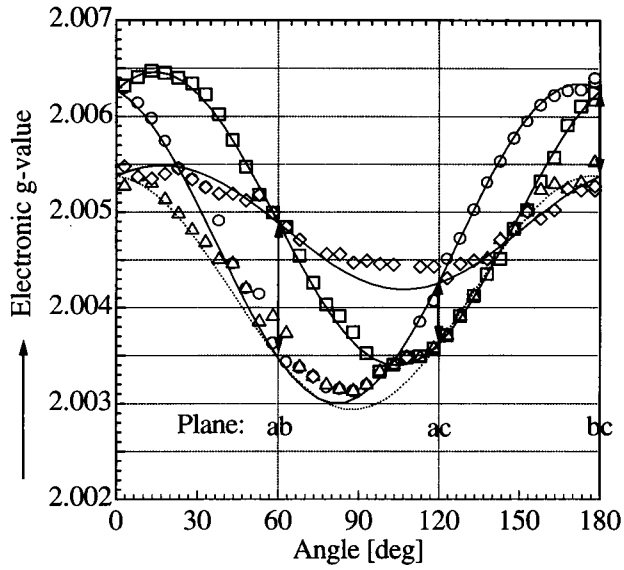

FIGURE 7 Experimental angular dependence of the g-factor of Q_A^- in Zn-bRC single crystals at 80 K for rotation of the magnetic field in the (1,1,1)-plane connecting the maximal site splittings (45° or 135°) of the three symmetry planes *a-b*, *a-c*, and *b-c*. For crystal orientation and mounting see text and Fig. 2. The symbols ○, △, ◇, and □ represent the experimental patterns for sites 1 to 4, respectively, in the crystal. Solid and dotted curves are calculated patterns for tensor set A (see Fig. 6 *A*).

Fig 1), is most sensitive to environmental effects influencing the surrounding of the oxygen atoms (lone pairs). Possible reasons for the difference between Q_A^- and Q_B^- is the more polar environment of Q_B and the accessibility of water molecules to this site as compared with the more apolar Q_A site. According to Stone, (1963) the dominant contribution to the g-shift Δg_{xx} ($\Delta g_{xx} = g_{xx} - 2.00232$) originates from the excitation of an electron in the nonbonding lone pair n-orbitals of the oxygen atoms into the half-occupied π^*-orbital. The magnitude of Δg_{xx} is inversely proportional to the energy gap between these two orbitals. Formation of hydrogen bonds to the n-orbitals is expected to increase this energy gap thereby decreasing Δg_{xx}, whereas π-interactions with surrounding aromatic amino acid residues are expected to decrease the energy gap and increase Δg_{xx}. The observed larger values of g_{xx} for Q_A^- may arise from weaker (or asymmetric) hydrogen bonding and/or from π-interaction with the aromatic environment of Q_A (e.g., close distance to tryptophan M252; Allen et al., 1988). The lower g_{xx} values for Q_B^- may be attributed to stronger hydrogen bonds and/or to the more polar environment of Q_B, which prevents π-interactions. These values are similar to those for UQ_{10}^- in frozen isopropanol. It has been shown for the duroquinone anion radical that changing the solvent from isopropanol to methyl tetrahydrofuran, which is less polar and not capable of forming hydrogen bonds, shifts the component g_{xx} from 2.0061 to 2.0067 (Burghaus et al., 1993).

Comparison of the g-tensors of Q_A^- in Zn-bRC single crystals at 80 K and 275 K reveals small differences for both the principal values and the principal axes (Table 3). This may be explained by an increased mobility of the six-membered ring of Q_A at elevated temperatures. As this ring is connected to the protein by hydrogen bonds at each of the carbonyl oxygens (Chirino et al., 1994; Ermler et al., 1994), the major type of motion is expected to be a rotational oscillation around the axis connecting the two oxygens. This motion should increase the magnitude of g_{zz} and decrease g_{yy}. The value of g_{xx} should not be affected (partial motional averaging in the *yz* plane). Indeed, g_{zz} is larger at 275 K as compared with g_{zz} at 80 K (Table 4), although g_{yy} remains constant and g_{xx} is increased at 275 K. The increased value of g_{xx} may indicate weaker hydrogen bonds at higher temperature, which is expected to decrease the energy gap between the oxygen lone pair n-orbitals and the half-filled π^*-orbital (see above). This should also lead to a slight increase of g_{yy} resulting from the motion about the *x* axis. The angles between corresponding principal axes (g_{xx}, g_{yy}, and g_{zz}) at 80 K and 275 K deviate only by 2°, 6°, and

TABLE 3 Direction cosines and principal values of the electronic g-tensor of Q_A^- at 80 K and at 275 K in Zn-bRCs from *Rb. sphaeroides* R-26

Temperature		g-Tensor axes	Direction cosines[a] (i = x, y, z) ℓ_{ia}	ℓ_{ib}	ℓ_{ic}	g-Tensor principal values
80 K	g_1	g_{xx}	**−0.18 (3)**	**0.85 (2)**	**0.50 (2)**	**2.00647 (5)**
		g_{yy}	**0.02 (7)**	**−0.50 (3)**	**0.86 (2)**	**2.00532 (5)**
		g_{zz}	**0.98 (1)**	**0.16 (2)**	**0.07 (4)**	**2.00218 (5)**
80 K	g_1*[b]	g_{xx}	−0.11 (3)	0.88 (2)	0.46 (2)	2.00638 (5)
		g_{yy}	0.18 (1)	−0.43 (3)	0.88 (2)	2.00544 (5)
		g_{zz}	0.98 (1)	0.18 (2)	−0.11 (4)	2.00215 (5)
275 K	g_1	g_{xx}	**−0.14**	**0.86**	**0.49**	**2.00652 (5)**
		g_{yy}	**−0.08**	**−0.51**	**0.86**	**2.00534 (5)**
		g_{zz}	**0.99**	**0.08**	**0.14**	**2.00238 (5)**
275 K	g_1*	g_{xx}	−0.03	0.89	0.46	2.00645 (5)
		g_{yy}	0.20	−0.45	0.87	2.00544 (5)
		g_{zz}	0.98	0.12	−0.16	2.00235 (5)

[a] Direction cosines in the crystal axis system (a, b, c) for tensors g_1 and g_1* assigned to Q_A^- site 1 (see Fig. 3 and Table 5). Tensors g_2, g_3, g_4 and g_2*, g_3*, g_4* have the same principal values and magnitudes of the direction cosines as g_1 and g_1*, respectively; only the signs of the direction cosines are different (see Table 2). Numbers in parentheses are errors in the last digit and correspond to errors of the orientation of the principal axes of ±3°. These numbers result from the errors of the g-tensor elements given in Table 1. The angles between corresponding eigenvectors (ℓ_{ia}, ℓ_{ib}, ℓ_{ic}) of tensors g_1 at 80 K and at 275 K are 2°, 6°, and 6° for i = x, y, and z, respectively.

[b] Tensor g_1* is obtained for a different combination of signs of the off-diagonal elements g_{ij} (see Table 2). From the experiments in the skew plane (1, 1, 1) g_1* can be eliminated (see text and Figs. 6 and 7).

6°, respectively, as calculated from the direction cosines given in Table 3. Hence there is no significant reorientation of Q_A^- upon freezing the RC single crystals.

From the observed difference in the low temperature recombination rates $D^+Q_A^- \rightarrow DQ_A$ in bRCs frozen in the light and in the dark, Kleinfeld et al. (1984) proposed light-induced structural changes in the bRC. More recently it has been discussed, on the basis of the x-ray structure analysis, that Q_A might move upon one electron reduction and that this displacement may facilitate electron transfer to Q_B (Allen et al., 1988). This question may be addressed by comparing the orientation of reduced Q_A^- with that of unreduced Q_A. The orientation of Q_A is obtained from the x-ray structure analysis and of Q_A^- from the orientation of the g-tensor axes, which is assumed to be related to the molecular axes as shown in Fig. 1. We start by examining the justification of this assumption.

For an isolated benzoquinone anion radical it has been shown experimentally that the g-tensor axes are colinear with the molecular axes. The axis of the g-tensor having the

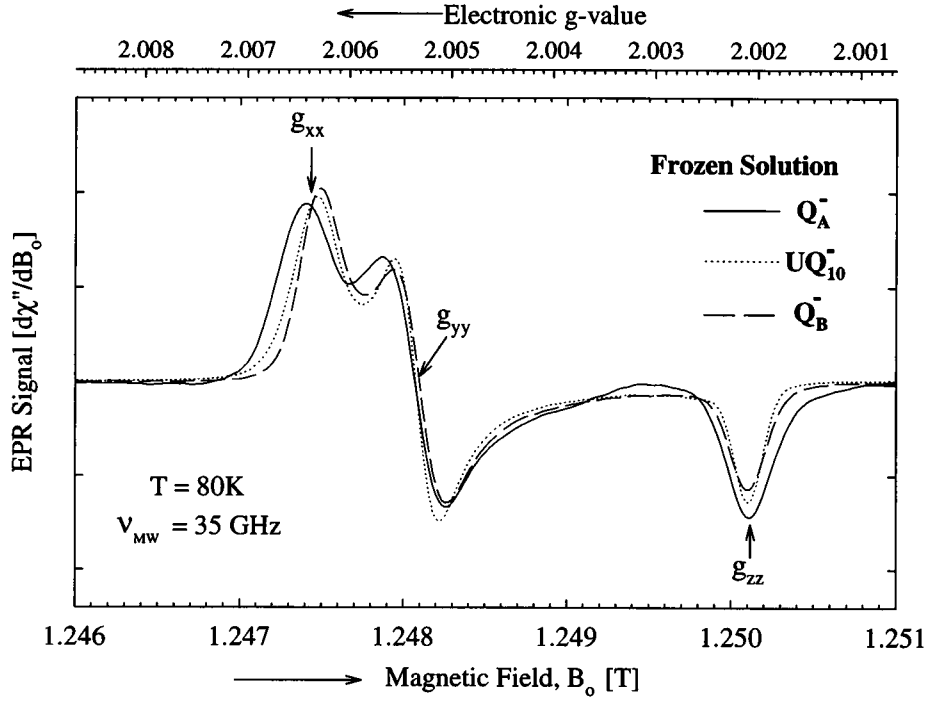

FIGURE 8 Q-band (35 GHz) powder EPR spectra of perdeuterated UQ_{10}^- in isopropanol-d_8 and of Q_A^- and Q_B^- in fully deuterated Zn-bRCs (D_2O buffer). Experimental conditions: microwave power = 0.3 μW; field modulation amplitude = 0.2 mT and frequency = 400 Hz; scan time = 30 s, 16 scans each; T = 80 K.

TABLE 4 Principal values of electronic g-tensors of Q_A^- in Zn-bRC single crystals and of Q_A^-, Q_B^-, and UQ_{10}^- in frozen solutions[a]

	Q_A^- Zn-bRC single crystals		Q_A^- frozen Zn-bRCs		Q_B^- frozen Zn-bRCs	UQ_{10}^-	
		This work[b]	This work,[c]	Burghaus et al., 1993,[d]	This work[e]	This work[f]	Burghaus et al., 1993,[g]
	275 K	80 K	80 K	80 K	80 K	130 K	130 K
g_{xx}	2.00652 (5)	2.00647 (5)	2.00649 (5)	2.0066 (1)	2.00626 (5)	2.00632 (5)	2.00646 (5)
g_{yy}	2.00534 (5)	2.00532 (5)	2.00532 (5)	2.0054 (1)	2.00527 (5)	2.00533 (5)	2.00542 (5)
g_{zz}	2.00238 (5)	2.00218 (5)	2.00210 (5)	2.0022 (1)	2.00213 (5)	2.00215 (5)	2.00222 (5)

[a] Numbers in parentheses are errors in the last digit.
[b] Q-band (35 GHz), Q_A replaced by perdeuterated UQ_{10}. Q_A^- generated by dithionite reduction (see text). Principal values of tensors set A (g_1–g_4), see Tables 2 and 3.
[c] Q-band, Q_A replaced by perdeuterated UQ_{10}. Q_A^- generated by continuous wave illumination of Zn-bRCs in the presence of reduced cytochrome *c*.
[d] W-band (95 GHz), Q_A^- in Zn-bRCs of Rb. sphaeroides R-26, generated by dithionite reduction.
[e] Q-band, Q_B replaced by perdeuterated UQ_{10}. Q_B^- generated by one saturating laser flash in dark-adapted Zn-bRCs in the presence of reduced cytochrome *c*.
[f] Q-band, perdeuterated UQ_{10}^- in alkaline isopropanol-d_8.
[g] W-band, UQ_{10}^- in alkaline isopropanol.

smallest principal value (g_{zz}) is oriented perpendicular to the quinone plane (*z* axis), the axis of the largest value (g_{xx}) is along the line connecting the two carbonyl groups (*x* axis), and the axis of the third principal value is perpendicular to the carbonyl-carbonyl axis lying in the quinone plane (*y* axis) (Burghaus et al., 1993; see Fig. 1). To investigate whether this is also the case for UQ_{10}^- and if a rotation of the g-tensor axes can possibly be induced by effects of the protein, e.g., by hydrogen bonds, we have performed g-tensor calculations on Q_A^-, based on the x-ray structure (Allen et al., 1988) using RHF/INDO wave functions and a parameterized form of Stone's equation as described by Burghaus et al. (1993). The calculated g_{xx} axis using the bare x-ray structure of Q_A was found to be rotated out of plane from the direction of the O1-O4 axis by only 2°. The g_{yy} and g_{zz} axes coincided within 1° with the molecular *y* and *z* axes of Q_A (see Fig. 1). The small deviation of g_{xx} from the molecular axis is probably caused by slight deviations of the x-ray structure of Q_A from standard geometry. Introduction of two hydrogen bonds (one to each carbonyl group), simulated by point charges (+0.5e) at 1.8 Å distance along either of the oxygen lone-pair orbital directions (dashed lines in Fig. 1), resulted in a decrease of the g_{xx} value by 0.0001. The effect of the point charges on the g-tensor axes orientations was, however, less than 1° in all cases. Replacement of the point charge by a water molecule placed in the Q_A plane with the (quinone) O ... H-O (water) axis along the Q_A oxygen lone-pair axis and an O . . . H distance of 1.5 Å resulted in qualitatively and quantitatively similar effects to those of a point charge (+0.5e) in place of the hydrogen atom. The calculations therefore suggest that even in cases of asymmetrically oriented hydrogen bonds, the g-tensor axes are very close to the molecular axes of Q_A^- shown in Fig 1.

To obtain the orientations of the principal axes of the g-tensor in the crystal, the four g-tensors g_1–g_4 (Tables 2 and 3) must be assigned to the four sites of Q_A^- in the crystal unit cell (Fig. 3). We based this assignment on the assumption of minimal changes of the orientation of Q_A^- as compared with the x-ray structure of Q_A. Table 5 gives the

TABLE 5 Angles (degrees) between principal axes of tensors g_1, g_2, g_3, and g_4 and the Q_A molecular axes (*x*, *y*, *z*)[a] for two different crystal structure determinations

	Angles[c]						
	T = 275 K			T = 80 K			
Tensor[b]	*x*, g_{xx}	*y*, g_{yy}	*z*, g_{zz}	*x*, g_{xx}	*y*, g_{yy}	*z*, g_{zz}	Reference
g_1	7	4	8	9	1	9	Chirimo et al., 1994;
g_2	61	62	9	62	61	10	Brookhaven PDB
g_3	61	62	9	62	61	11	entry 1PSS
g_4	9	4	10	11	1	11	
g_1	14	14	17	16	9	15	Ermler et al., 1994;
g_2	68	67	4	68	68	9	Brookhaven PDB,
g_3	66	69	17	67	68	16	entry 1PCR
g_4	8	7	6	9	11	11	

[a] Angles with respect to Q_A of site 1 in the unit cell (see Fig. 3), for which the x-ray coordinates are given.
[b] Tensors g_1, g_2, g_3, and g_4 arising from the possible sign combinations of the off-diagonal elements, g_{ij} (see Table 1), and representing the four sites in the crystal unit cell. Tensor g_1 is assigned to Q_A^- of site 1.
[c] Angles between molecular axes *x*, *y*, *z* of Q_A and the principal axes of the g-tensor, g_{xx}, g_{yy}, and g_{zz}, respectively; estimated errors of principal axes are ±3° (see text and Table 3). For all angles >90° (obtained using the direction cosines and signs of Tables 2 and 3) the complementary values to 180° are given.

angles between the four sets of eigenvectors (tensors g_1, g_2, g_3, and g_4) for 80 K and for 275 K and the molecular axis system of Q_A of site 1 as obtained from the recent x-ray structures of Chirino et al. (1994) and Ermler et al. (1994). In the former case the smallest angles between the g-tensor and molecular axes are obtained when tensor g_1 is assigned to the x-ray coordinates of Q_A in site 1 (Fig. 3). In this case the g-tensor x axis is rotated by ~9° in the x-z plane with respect to the axis system of the neutral Q_A. Assignment of tensor g_4 to site 1 would imply a rotation of ~11°. For the second x-ray structure (Ermler et al., 1994), the smaller angles are obtained when tensor g_4 is assigned to site 1. It is therefore not possible to distinguish between these two assignments on the basis of these two sets of x-ray data.

Table 6 gives the angles between the principal axes of the g-tensor g_1 and the molecular axes of Q_A (x, y, z) (see Fig. 1) obtained from four independent x-ray studies of *Rb. sphaeroides* R-26 and 2.4.1 bRCs (Allen et al., 1988; Chang et al., 1991; Chirino et al., 1994; Ermler et al., 1994). We do not expect a difference between the structure of the wild-type strain 2.4.1 and the carotenoidless mutant R-26 except in the vicinity of the carotenoid. For the cation radical of the primary donor it has been shown that the proton hyperfine tensor orientations, which are sensitive to structural changes, agree within ±2° in these two species (Gessner et al., 1992). As the carotenoid is at a larger distance from Q_A (approximately 30 Å) than from the donor, we do not expect a structural difference for the Q_A site between R-26 and 2.4.1. Comparison between the Q_A orientations in these two species shows, however, that there is a considerable difference of ~12° (see Fig. 3, *b*-*c* plane). As differences of comparable magnitude are also observed for the x-ray structures of the same species, they are attributed to errors arising from the limited resolution of the x-ray structure determination rather than to real differences between species. There is clearly a need for a more reliable, higher resolution x-ray structure.

The angles between corresponding g-tensor and molecular axes vary between 2° and 24° (Table 6). The deviations between the Q_A axes of the different x-ray structures (7° to 20°) show, however, a similar spread of values. The orientation of the g-tensor principal axes deviate by approximately 6° to 8° (80 K) and 4° to 12° (275 K) from the average Q_A orientation calculated from the four x-ray structures. These values are obtained when g_1 is assigned to site 1. The corresponding angles for assignment of g_4 to site 1 (see Table 5) are 8° to 17° for 80 K and 5° to 14° for 275 K (see Table 6, last column, and footnote *f*), which indicates a preference for the former assignment. Considering the experimental errors of the orientation of the g-tensor axes (±3°) and the spread between the orientations of the Q_A molecular axes obtained from the four x-ray studies (up to 20°), we do not consider the deviation between the g-tensor axes of Q_A^- and the molecular axes of Q_A to be significant. The relative orientations of the axes of the g-tensor of Q_A^- at 80 K (assigning g_1 to site 1) and of Q_A from the four x-ray structures are shown stereographically in Fig. 9.

The analysis of our data gives no indication for a reorientation of Q_A of more than 10° upon one electron reduction. However, it should be noted that we have biased our assignment by assuming a minimal change of the orientation of Q_A^- (see Table 5). Independent evidence for the lack of reorientation of Q_A^- was obtained from an analysis of spin-polarized EPR spectra of the radical pair state $D^+ Q_A^-$ in Zn-bRCs (van der Est et al., 1993) and from C-O vibrational frequencies from Fourier transform infrared spectroscopy (FTIR) (Breton et al., 1994a,b). How can we reconcile this result with the light-induced structural changes proposed by Kleinfeld et al. (1984)? One possibility is that a translational displacement of Q_A^-, which would not affect the orientation of the molecular axes (and therefore not show up in these experiments) takes place. An

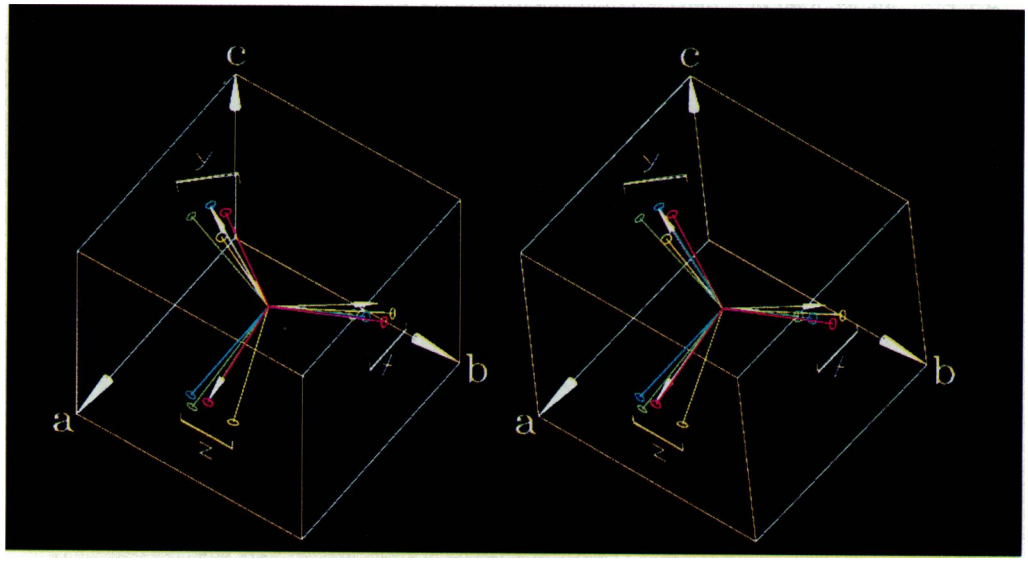

FIGURE 9 Stereo view of the axes directions (unit vectors) of the g-tensor of Q_A^- measured in this paper (80 K) and of Q_A (site 1) obtained from the four x-ray structures of *Rb. sphaeroides* (Allen et al., 1988; Chang et al., 1991; Chirino et al., 1994; Ermler et al., 1994). White is g-tensor g_1 (Table 3). Q_A axes: red is R-26 (Allen et al., 1988); blue is wild-type 2.4.1 (Chirino et al., 1994); green is wild-type 2.4.1 (Ermler et al., 1994, after proper rotation to account for the different crystal space groups); and yellow is R-26 (Chang et al., 1991). The axes of the cube are parallel to the axes a, b, and c of the unit cell of the orthorhombic crystals (Allen et al., 1988).

TABLE 6 Angles (degrees) between principal axes of the g tensor (g_1) and molecular axes of Q_A from different x-ray crystallographic studies of *Rb. sphaeroides* Zn-bRC single crystals

Tensor	Angles[a]	R-26[b]	Strain 2.4.1[c]	Strain 2.4.1[d]	R-26[e]	Vector average[f]
g_1	g_{xx}, x	8	7	14	13	4
(275 K)	g_{yy}, y	12	4	14	24	11
	g_{zz}, z	8	8	17	23	12
g_1	g_{xx}, x	9	9	16	12	6
(80 K)	g_{yy}, y	9	1	9	20	6
	g_{zz}, z	3	9	15	16	8

[a] Angles between g-tensor axes and molecular axes (x, y, z) of Q_A of site 1 (see Fig. 3). Errors of g-tensor principal axes ±3°.
[b] Brookhaven Protein Data Bank (PDB) entry 4RCR; see also Allen et al. (1988).
[c] Chirino et al. (1994), Brookhaven PDB entry 1PSS.
[d] Ermler et al. (1994), Brookhaven PDB entry 1PCR. This x-ray structure exhibits the highest resolution (2.65 Å) and is obtained on crystals with a different unit cell (space group $P3_12_1$). Angles were obtained after rotation of the x-ray coordinates to match the cofactor arrangement with those for the other structure with space group $P2_12_12_1$ crystals used for the EPR experiments (G. Fritzsch, private communication). This rotation may introduce an additional systematic error for the angle, which might explain the larger values obtained for this structure as compared with those for structures R-26 and strain 2.4.1.
[e] Brookhaven PDB entry 2RCR; see also Chang et al. (1991).
[f] Average orientation of Q_A from the four X-ray structures. If the same averages were taken assuming that g_4 corresponds to site 1, the numbers in this column would be 14°, 5°, 13°, 16°, 8°, and 17°, showing a preference for g_1 as site 1.

alternate possibility is that the structural changes occur at or near the site of D^+.

Another striking difference between the various x-ray structures is the distance between Q_A and Fe^{2+}, which differs by up to 1.5 Å. Consequently, different H-bonds are proposed for the Q_A carbonyl group (O4, Fig. 1) to His M219 in Chirino et al. (1994) and Ermler et al. (1994) and to Thr M222 in Allen et al. (1988). In a recent study by van den Brink et al. (1994), Q_A has been replaced by UQ_{10}, which was selectively enriched in ^{13}C either at the position C1 or C4 (see Fig. 1). EPR spectra of Q_A^- were measured at 35 GHz in frozen RC solutions. From the resolved different ^{13}C hyperfine couplings at positions C1 and C4 a stronger hydrogen bond was proposed to O4, and was tentatively assigned to His M219. Breton et al. (1994a) have done FTIR experiments that also show a stronger H-bond to O4. We have performed preliminary ENDOR experiments on Q_A^- in Zn-bRC single crystals of *Rb. sphaeroides*, where resonances from exchangeable protons could clearly be identified (Lubitz et al., 1993; Isaacson et al., 1995). Work is in progress to determine the orientation and distance of the protons in hydrogen bonds to the carbonyl oxygens. This may provide a more accurate way of determining the position of Q_A^- in the protein. EPR and ENDOR experiments on Q_A^-, in combination with NMR experiments on diamagnetic Q_A (Van Liemt et al., 1993) and FTIR (Buchanan et al., 1992; Breton et al., 1994a,b; Brudler et al., 1994), offer an alternative way for studying possible structural changes of Q_A after electron transfer.

We thank M. Plato (Freie Universität Berlin) for providing his RHF/INDO/SP program and for his advice in calculating the g-tensors, R. Bittl for his help concerning the comparison of the x-ray data, and R. Fiege (both Technische Universität Berlin) for providing the spectra simulation program. We thank G. Fritzsch and H. Michel (Max-Planck-Institut, Frankfurt), D. C. Rees (University of California, Los Angeles) and M. Schiffer (Argonne National Laboratory) for making x-ray coordinates available to us before publication, and G. Fritzsch also for providing the transformation matrix between the trigonal and orthogonal crystals.

This work was supported by grants from the National Science Foundation (MCB 89–15631), the National Institutes of Health (GM 13191), Deutsche Forschungsgemeinschaft (Sfb 312), and NATO (CRG 910468). W. Lubitz is grateful for financial support provided by the Fonds der Chemischen Industrie (Germany) and by Schering AG (Berlin).

REFERENCES

Allen, J. P., G. Feher, T. O. Yeates, H. Komiya, and D. C. Rees. 1988. Structure of the reaction center from *Rhodobacter sphaeroides* R-26: protein-cofactor (quinones and Fe^{2+}) interactions. *Proc. Natl. Acad. Sci. USA.* 85:8487–8491.

Allen, J. P., and G. Feher 1991. Crystallization of reaction centers from *Rhodobacter sphaeroides*. *In* Crystallization of Membrane Proteins. H. Michel, editor. CRC Press, Boca Raton, FL. 137–153.

Atherton, N. M. 1993. Principles of Electron Spin Resonance. Ellis Horwood and PTR Prentice Hall, New York. Chap. 4. 130–138.

Breton, J., C. Boullais, J.-R. Burie, E. Nabedryk, and C. Mioskowski. 1994a. Binding sites of quinones in photosynthetic bacterial reaction centers investigated by light-induced FTIR difference spectroscopy: assignment of the interactions of each carbonyl of Q_A in *Rhodobacter sphaeroides* using site-specific ^{13}C-labeled ubiquinone. *Biochemistry.* 33:14378–14386.

Breton, J., J.-R. Burie, C. Berthomieu, G. Berger, and E. Nabedryk. 1994b. The binding sites of quinones in photosynthetic bacterial reaction centers investigated by light-induced FTIR difference spectroscopy: assignment of the Q_A vibrations in *Rhodobacter sphaeroides* using ^{18}O- or ^{13}C-labeled ubiquinone and vitamin K_1. *Biochemistry.* 33:4953–4965.

Brudler, R., H. J. M. de Groot, W. B. S. van Liemt, W. F. Steggerda, R. Esmeijer, P. Gast, A. J. Hoff, J. Lugtenburg and K. Gerwert. 1994. Asymmetric binding of the I- and 4-C=O groups of Q_A in *Rhodobacter sphaeroides* R26 reaction centres monitored by Fourier transform infrared spectroscopy using site-specific isotopically labelled ubiquinone-10. *EMBO J.* 13:5523–5530.

Buchanan, S. K., and G. C. Dismukes. 1987. Substitution of Cu^{2+} in the reaction center diquinone electron acceptor complex of *Rhodobacter sphaeroides*: determination of the metal-ligand coordination. *Biochemistry.* 26:5049–5055.

Buchanan, S., H. Michel, and K. Gerwert. 1992. Light-induced charge separation in *Rhodopseudomonas viridis* reaction centers monitored by fourier-transform infrared difference spectroscopy: the quinone vibrations. *Biochemistry.* 31:1314–1322.

Burghaus, O., M. Plato, M. Rohrer, K. Möbius, F. MacMillan, and W. Lubitz. 1993. 3-mm high-field EPR on semiquinone radical anions Q^- related to photosynthesis and on the primary donor P^+ and acceptor Q_A^- in reaction centers of *Rhodobacter sphaeroides* R-26. *J. Phys. Chem.* 97:7639–7647.

Butler, W. F., R. Calvo, D. R. Fredkin, R. A. Isaacson, M. Y. Okamura, and G. Feher. 1984. The electronic structure of Fe^{2+} in reaction centers from *Rhodopseudomonas sphaeroides*. III. EPR measurements of the reduced acceptor complex. *Biophys. J.* 45:947–973.

Carrington, A., and A. D. McLachlan. 1969. Introduction to Magnetic Resonance. Harper and Row, New York. Chap. 9.

Chang, C.-H., El-Kabani, O., Tiede, D., Norris, J., and Schiffer, M. 1991. Structure of the membrane-bound protein photosynthetic reaction center from *Rhodobacter sphaeroides*. *Biochemistry.* 30:5352–5360.

Chirino, A. J., E. J. Lous, M. Huber, J. P. Allen, C. C. Schenck, M. L. Paddock, G. Feher, and D. C. Rees. 1994. Crystallographic analysis of site-directed mutants of the photosynthetic reaction center from *Rhodobacter sphaeroides*. *Biochemistry.* 33:4584–4593.

Debus, R. J., G. Feher, and M. Y. Okamura. 1986. Iron-depleted reaction centers from *Rhodopseudomonas sphaeroides* R26.1: characterization and reconstitution with Fe^{2+}, Mn^{2+}, Co^{2+}, Ni^{2+}, Cu^{2+}, and Zn^{2+}. *Biochemistry.* 25:2276–2287.

Deisenhofer, J., and H. Michel. 1989. The photosynthetic reaction centre from the purple bacterium *Rhodopseudomonas viridis*. *EMBO J.* 8:2149–2170.

Ermler, U., G. Fritzsch, S. K. Buchanan, and H. Michel. 1994. Structure of the photosynthetic reaction centre form *Rhodobacter sphaeroides* at 2.65 Å resolution: cofactors and protein-cofactor interactions. *Structure.* 2:925–936.

Feher, G., J. P. Allen, M. Y. Okamura, and D. C. Rees. 1989. Primary processes in bacterial photosynthesis: structure and function of reaction centers. *Nature.* 339:111–116.

Feher, G., R. A. Isaacson, M. Y. Okamura, and W. Lubitz. 1985. ENDOR of semiquinones in reaction centers from *Rhodopseudomonas sphaeroides*. *In* Antennas and Reaction Centers of Photosynthetic Bacteria. Michel-Beyerle, editor. Springer Verlag, Berlin. 174–189.

Feher, G., and M. Y. Okamura. 1978. Chemical composition and properties of reaction centers. *In* The Photosynthetic Bacteria. R. K. Clayton and W. R. Sistrom, editors. Plenum Press, New York. 349–386.

Feher, G., M. Y. Okamura, and J. D. McElroy. 1972. Identification of an electron acceptor in reaction centers of *Rhodopseudomonas sphaeroides* by EPR spectroscopy. *Biochim. Biophys. Acta.* 267:222–226.

Ferris, K. 1987. Metals in catalysis and electron transfer. PhD Thesis. Princeton University, Princeton, NJ. 139–143.

Gessner, C., F. Lendzian, B. Bönigk, M. Plato, K. Möbius, and W. Lubitz. 1992. Proton ENDOR and TRIPLE resonance investigation of P_{865}^+ in Photosynthetic Reaction Center Single Crystals of *Rb. sphaeroides* wild type 2.4.1. *Appl. Magn. Reson.* 3:763–777.

Isaacson, R. A., E. C. Abresch, G. Feher, F. Lendzian, and W. Lubitz. 1994. EPR studies at 35 GHz of Q_A^- in single crystals of reaction centers from *Rb. sphaeroides*. *Biophys. J.* 66:A229.

Isaacson, R. A., E. C. Abresch, G. Feher, W. Lubitz, J. C. Williams, and J. P. Allen. 1995. ENDOR studies of Q_A^- in single crystals of reaction centers from *Rb. Sphaeroides*. *Biophys. J.* 68:A246.

Kirmaier, C., D. Holten, R. J. Debus, G. Feher, and M. Y. Okamura. 1986. Primary photochemistry of iron-depleted and zinc-reconstituted reaction centers from *Rhodopseudomonas sphaeroides*. *Proc. Natl. Acad. Sci. USA.* 83:6407–6411.

Kleinfeld, D., M. Y. Okamura, and G. Feher 1984. Electron-transfer kinetics in photosynthetic reaction centers cooled to cryogenic temperatures in the charge-separated state: evidence for light-induced structural changes. *Biochemistry.* 23:5780–5786.

Klette, R., J. T. Törring, M. Plato, K. Möbius, B. Bönigk, and W. Lubitz. 1993. Determination of the g-tensor of the primary donor cation radical in single crystals of *Rhodobacter sphaeroides* R-26 reaction centers by 3-mm high-field EPR. *J. Phys. Chem.* 97:2015–2020.

Loach, P. A., and R. L. Hall. 1972. The question of the primary electron acceptor in bacterial photosynthesis. *Proc. Natl. Acad. Sci. USA.* 69:786–790.

Low, W. 1957. Paramagnetic resonance spectrum of manganese in cubic MgO and CaF_2. *Phys. Rev.* 105:793–800.

Lubitz, W., E. C. Abresch, R. J. Debus, R. A. Isaacson, M. Y. Okamura, and G. Feher. 1985. Electron nuclear double resonance of semiquinones in reaction centers of *Rhodopseudomonas sphaeroides*. *Biochim. Biophys. Acta.* 808:464–469.

Lubitz, W., R. A. Isaacson, E. C. Abresch, and G. Feher. 1993. EPR and ENDOR studies of Q_A^- in reaction center single crystals from *Rb. sphaeroides* R-26 in which iron was replaced by zinc. *Biophys. J.* 64:A18.

Okamura, M. Y., R. J. Debus, D. Kleinfield, and G. Feher. 1982. Quinone binding sites in reaction centers from photosynthetic bacteria. *In* Function of Quinones in Energy Conserving Systems. B. L. Trumpower, editor. Academic Press, New York. 299–317.

Okamura, M. Y., R. A. Isaacson, and G. Feher. 1975. The primary acceptor in bacterial photosynthesis: the obligatory role of ubiquinone in photoactive reaction centers of *Rhodopseudomonas sphaeroides*. *Proc. Natl. Acad. Sci. USA.* 72:3491–3495.

Okamura, M. Y., and G. Feher. 1992. Proton transfer in reaction centers from photosynthetic bacteria. *Annu. Rev. Biochem.* 61:861–896.

Pederson, J. A. 1983. Handbook of EPR Spectra from Quinones and Quinols. CRC Press, Boca Raton, FL. 67–73.

Press, W. H., B. P. Flannery, S. A. Teukolsky, and W. T. Vetterling. 1988. Numerical Recipes in C: The Art of Scientific Computing. Cambridge University Press, New York.

Rieger, P. H. 1982. Least-squares analysis of ESR powder patterns with noncoincident principal axes of the g and hyperfine tensors. *J. Magn. Reson.* 50:485–489.

Rutherford, A. W., I. Agalidis, and F. Reiss-Husson. 1985. Manganese-quinone interactions in the electron acceptor region of bacterial photosynthetic reaction centres. *FEBS Lett.* 182:151–157.

Schelvis, J. P. M., B.-L. Liu, T. J. Aartsma, and A. J. Hoff. 1992. The electron transfer rate from Bph_A^- to Q_A in reaction centers of *Rb. sphaeroides* R-26: influence of the H-subunit, the Q_A and Fe^{2+} cofactors and the isoprenene tail of Q_A. *Biochim. Biophys. Acta.* 1102:229–236.

Shinkarev, V. P., and C. A. Wraight. 1993. Electron and proton transfer in the acceptor quinone complex of reaction centers of phototrophic bacteria. *In* The Photosynthetic Reaction Center, Vol. 1. J. Deisenhofer and J. R. Norris, editors. Academic Press, San Diego. 193–255.

Stesmans, A., and G. De Vos. 1986. ESR observation of temperature-dependent g-shifts in submetallic P-doped Si at low temperatures. *Phys. Rev. B.* 34:6499–6502.

Stesmans, A., and G. Van Gorp. 1989. Novel method for accurate g measurements in electron-spin resonance. *Rev. Sci. Instr.* 60:2949–2952.

Stone, A. J. 1963. g-factors in aromatic free radicals. *Mol. Phys.* 6:509–515.

Takamiya, K., and A. Takamiya. 1969. Light-induced reactions of ubiquinone in photosynthetic bacterium, *Chromatium D.* III. Oxidation-reduction state of ubiquinone in intact cells of *Chromatium D. Plant Cell Physiol.* 10:363–373.

van den Brink, J. S., A. P. Spoyalov, P. Gast, B. S. W. van Liemt, J. Raap, J. Lugtenburg, and A. J. Hoff. 1994. Asymmetric binding of the primary acceptor quinone in reaction centers of the photosynthetic bacterium *Rb. sphaeroides* R-26, probed with Q-band (35 GHz) EPR spectroscopy. *FEBS Lett.* 353:273–276

van der Est, A., R. Bittl, E. C. Abresch, W. Lubitz, and D. Stehlik. 1993. Transient EPR spectroscopy of perdeuterated Zn-substituted reaction centres of *Rhodobacter sphaeroides* R-26. *Chem. Phys. Lett.* 212:561–568.

van Liemt, W. B. S., G. J. Boender, P. Gast, A. J. Hoff, J. Lugtenburg, and H. J. M. de Groot. 1993. Solid state magic angle spinning ^{13}C NMR spectroscopy of the Q_A binding site in *Rhodobacter sphaeroides* reaction centers, reconstituted with specifically ^{13}C-enriched ubiquinone-10. *Photochem. Photobiol.* 57:32S.

Wraight, C. A., 1979. Electron acceptors of bacterial photosynthetic reaction centers. II. H^+ binding coupled to secondary electron transfer in the quinone acceptor complex. *Biochim. Biophys. Acta.* 548:309–327.